Journal of Solid State Chemistry **160,** 272–277 (2001)
doi:10.1006/jssc.2001.9245, available online at http://www.idealibrary.com on IDEAL®

Defects and Photoluminescence of Ni^{2+} and Mn^{2+}-Doped Sol–Gel SiO_2 Glass

Ping Yang,* Chun Feng Song,* Meng Kai Lü,*,[1] Jun Chang,† Ying Zi Wang,† Zhong Xi Yang,† Guang Jun Zhou,‡ Zi Ping Ai,§ Dong Xu,* and Duo Long Yuan*

*State Key Laboratory of Crystal Material, Shandong University, Jinan 250100, People's Republic of China; †Shandong Institute of Building Materials, Jinan 250022, People's Republic of China; ‡Shandong Supervision and Inspection Institute for Product Quality, Jinan 250100, People's Republic of China; and §The Experimental Center of Shandong University, Jinan 250100, People's Republic of China

Received January 25, 2001; in revised form May 2, 2001; accepted May 11, 2001; published online June 29, 2001

SiO_2 glass doped with Ni^{2+} and Mn^{2+} has been prepared by the sol–gel process. Very strong visible light (its fluorescence efficiency is about 4 times of that of undoped sol–gel SiO_2 glass and about 160 times of that of ZnS nanocrystallites) from the SiO_2 glass doped with Ni^{2+} and Mn^{2+} has been observed. The emission wavelength of Ni^{2+}-doped, Mn^{2+}-doped, and undoped glass samples is about 450 nm. However, the co-doping of Ni^{2+} and Mn^{2+} shifts the emission wavelength to 420 nm. The sol–gel SiO_2 glass is a porous phosphor material. Very strong photoluminescence of the sol–gel SiO_2 glass mainly comes from structural defects. Because the doped samples contain more Si dangling bonds, nonbridging oxygen, and oxygen vacancy in its structure and surface defects inside the nanometer-scale hole in the sol–gel SiO_2 glass than undoped glass sample, the fluorescence efficiency of doped samples has been remarkably increased. Because the doped ions affect the band gap structure of the host materials, the emission wavelength of the co-doped samples is different from that of Ni^{2+}- and Mn^{2+}-doped samples. Because the emission wavelength of Ni^{2+} and Mn^{2+} luminescent centers in the sol–gel silica glass is almost the same as that of undoped sample, the fluorescence intensities of Ni^{2+}- and Mn^{2+}-doped samples are higher than those of the co-doped samples.

Key Words: **sol–gel; SiO_2 glass; luminescence; Ni^{2+}; Mn^{2+}; dope; defect.**

INTRODUCTION

The sol–gel technique has been used to prepare silicate glass with a wide range of unusual properties. It is widely used for optical materials, resistance film, passivation film, and so on (1–5). Also, it is a new class of stable, efficient, and environmentally friendly photoluminescence (PL) materials, a less toxic alternative, and leads to higher net conversion efficiency (3). In addition, the applications of sol–gel SiO_2 glass materials are easier and more convenient than those of other luminescent materials (for example II–VI and III–V luminescent materials). A great deal of work has been done over two decades to identify the formation and properties of the defects responsible for the ultraviolet (UV) PL in SiO_2-based glassy materials (10–12). This was mainly motivated by technological implications of PL defects in the physical properties of SiO_2-based devices for fiber optics.

Integrated optics is becoming increasingly important in modern telecommunications technology. One important field of research is the study of rare-earth-doped solid-state planar optical amplifiers. There are many reports of synthesizing visible PL rare-earth-doped sol–gel silica glass (6–9). Here, we present a very strong visible light from the sol–gel SiO_2 glass doped with Ni^{2+} and Mn^{2+} for the first time. We also discuss the luminescence mechanism of complex defects in the sol–gel SiO_2 glass doped with Ni^{2+} and Mn^{2+}.

EXPERIMENT

SiO_2 glass samples were prepared by sol–gel hydrolysis and condensation of $Si(OC_2H_5)_4$ in H_2O–ethanol solution. Reagent amounts were 10 ml of $Si(OC_2H_5)_4$, 7 ml of ethanol, and 15 ml of H_2O. HCl was a catalyst. The solution of ethanol, H_2O, and $Si(OC_2H_5)_4$ were mixed and stirred for 1 h at room temperature (T). Ni^{2+} and Mn^{2+} ions were added in the sol samples by using a solution of manganese chloride ($MnCl_24H_2O$) and nickel sulfate ($NiSO_46H_2O$) at 0.5 M. The sol was kept at room temperature until complete gelation. Final the xerogel was obtained in 1 week at room temperature. The xerogel samples were then heated in an ambient atmosphere at a rate of 10°C/h up to 50°C and kept for 10 h at 50°C. Some samples heat-treated at 50°C were then heated in an ambient atmosphere at a rate of 10°C/h up to 500°C and kept for 5 h at 500°C.

[1] To whom correspondence should be addressed. Fax: +86-531-8565403. E-mail: mklu@263.net.

0022-4596/01 $35.00

The purity of $Si(OC_2H_5)_4$ is CP (chemical pure). The purity of other reagents is GR (guaranteed reagent). ZnS nanocrystallines were synthesized as free-standing powder using the chemical precipitation method. In principle, the method adopted here is similar to that describe by R. Vacassy *et al.* (13)

A Hitachi (Japan) M-850 fluorescence spectrophotometer was used to measure the photoluminescence of the samples. Ideal spectral data were recorded with the slits set at 10 nm. First, the excitation wavelength was measured. The emission spectra of the samples were then recorded. For collecting the emission spectrum of ZnS nanoparticles, 25 mM colloidal solutions of ZnS nanocrystallites were obtained by dispersing ZnS nanoparticles in isopropyl alcohol. The absorption spectra of the samples were recorded by using a U-3500 spectrophotometer.

X-ray powder diffraction (XRD) patterns were recorded using a Rigaku (Japan) D/max-rA X-ray diffractometer with Cu$K\alpha$ irradiation ($\lambda = 1.5418$ Å) at 40 kV/100 mA. A secondary graphite crystal monochromator was used. The FTIR spectra of samples were collected using a 5DX Fourier transform infrared spectrometer. The DTA curve of the sample was recorded by conducting a NeTZSCH (Germany) STA 409 EP simultaneous thermal analysis in N_2 atmosphere.

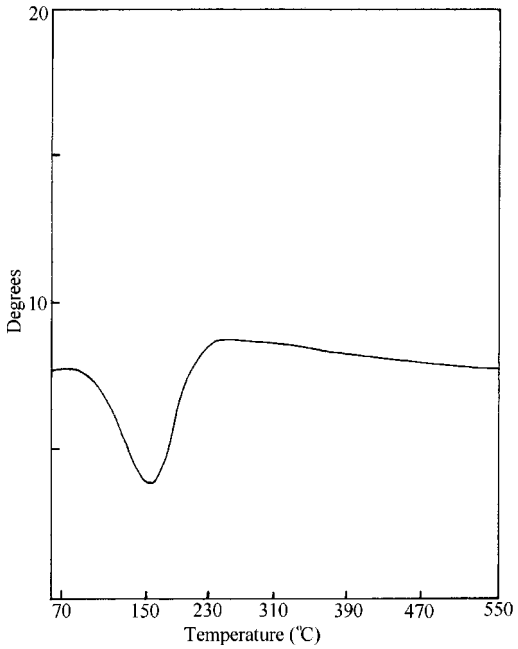

FIG. 2. DTA curve of the glass xerogel.

RESULTS AND DISCUSSION

Figure 1 shows the XRD patterns of the sample co-doped with Ni^{2+} and Mn^{2+} (Ni^{2+} doped 0.3%, Mn^{2+} doped 2.0% mole ratio) heat-treated at 500°C. The XRD pattern reveals a noncrystalline structure. Figure 2 shows DTA analysis of the undoped glass xerogel sample. DTA data indicate an endothermic reaction at 150°C, due to dehydration and rudimental ethanol.

Figure 3 shows the FTIR spectra of the SiO_2 xerogel and 500°C heat-treated samples. The FTIR spectrum of 500°C heat-treated samples is similar to the spectrum of pure amorphous SiO_2 (3). Strong bands associated with Si–O streching and bending vibrations are apparent at 1090, 800, and 470 cm^{-1}. The absorption at 3443 cm^{-1} indicates the presence of hydroxy (presence of H_2O). Additional weak absorptions at the 1640 and 960 cm^{-1} indicate the presence of oxyethyl.

Figure 4 shows the absorption spectra of the doped and undoped sol–gel glass samples. The absorption spectrum of the doped sample is remarkably different from that of the undoped sample. Due to the effect of doped ions on the band gap structure of the host materials, the absorption shoulder peak and absorption edge of the doped samples

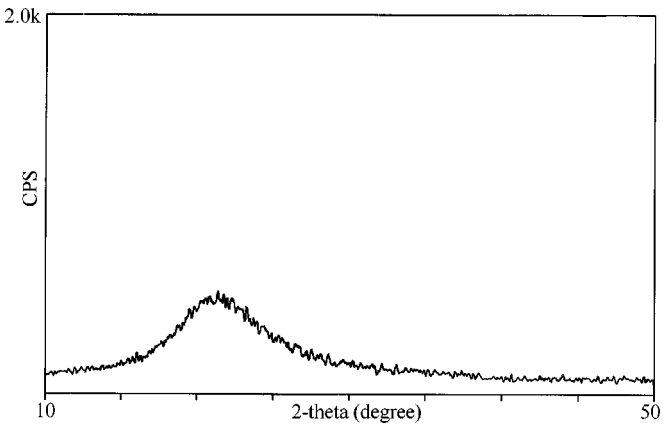

FIG. 1. XRD pattern of co-doped sample heat-treated at 500°C.

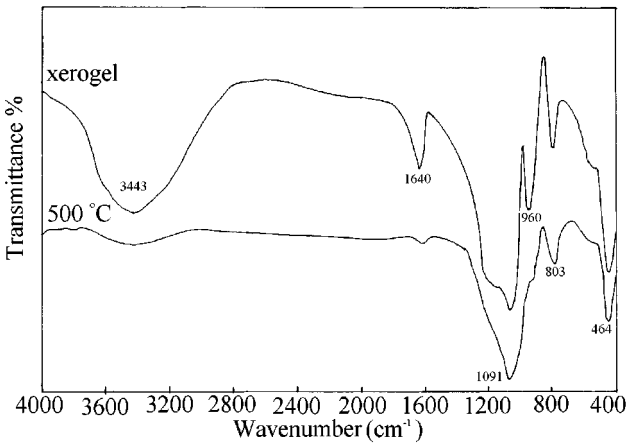

FIG. 3. FTIR spectra of the samples.

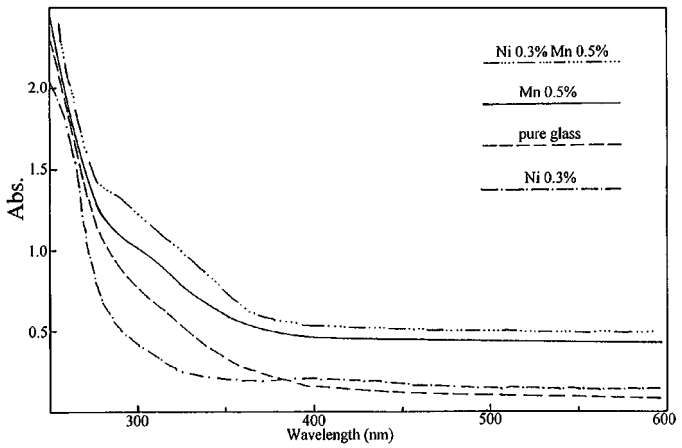

FIG. 4. Absorption spectra of the samples.

vary with the changes of doped ions. The absorption spectra of the doped and undoped samples occupy only an absorption band. Because the absorption spectra of the sol–gel glass samples do not vary with varying the impurity mole ratio of doped ions, the exciting spectra of all heat-treated samples are almost at the same position.

Figure 5 shows the excitation spectrum of the undoped silica xerogel. The excitation spectra of the doped samples are almost the same as those of the undoped sample. The fluorescent analysis of the samples shows that the excitation spectrum of doped and the undoped samples has an excitation band. The maximum value of the excitation band is 380 nm.

Figure 6 shows the emission spectrum of pure ZnS nanoparticles ($\lambda_{ex} = 350$ nm, $\lambda_{em} = 450$ nm). Figure 7 shows the emission spectrum of pure glass samples ($\lambda_{ex} = 380$ nm, $\lambda_{em} = 450$ nm). The relative fluorescence intensity of pure glass xerogel is about 40 times of that of ZnS nanocrystallites (the average size of ZnS nanometer crystal particles, estimated from the Debye–Scherrer formula, is ~ 2.4 nm). Thus, the sol–gel silica glass is a highly luminescent material compared with II–VI nanometer-scale semiconductor luminescent materials. The applications of the silica sol–gel silica glass are more convenient than those of other luminescent materials. Thus, the doped sol–gel silica glass changes into a new class of luminescent material.

Figure 8 shows the emission spectra of Ni-doped glass samples heat-treated at 50°C ($\lambda_{ex} = 380$ nm). All of the samples show that the emission peaks are almost at the same position ($\lambda_{em} = 450$ nm). The relative fluorescence intensity of the Ni^{2+}-doped glass sample (when impurity mole ratio of Ni is 0.3%) is about 4 times of that of the undoped SiO_2 glass sample. The fluorescence intensity of Ni-doped samples varies with increasing Ni-doped mole ratio. Ni^{2+} enhances remarkably the fluorescence intensity of the sol–gel glass.

Figure 9 shows the emission spectra of Mn-doped glass samples heat-treated at 50°C ($\lambda_{ex} = 380$ nm). All of the samples show the emission peaks almost at the same position ($\lambda_{em} = 450$ nm). The relative fluorescence intensity of the Mn-doped glass sample (when impurity mole ratio of Mn is 0.5%) is about 4 times of that of an undoped SiO_2 glass sample. The effect of Mn^{2+} on the fluorescence characteristics of the sol–gel glass is almost the same as that of Ni^{2+}. For luminescent materials, excessive impurities in the host materials can lead to formation of the deep trap center of the doped ion (21). Because the deep trap centers can trap electrons or holes in luminescence processes and lead to fluorescence quenching, the nonradiative combinations of

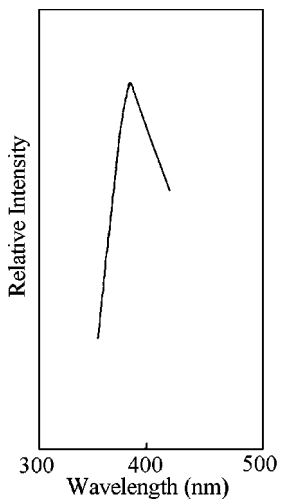

FIG. 5. Excitation spectrum of the undoped silica glass sample (heat-treated at 50°C, $\lambda_{em} = 450$ nm)

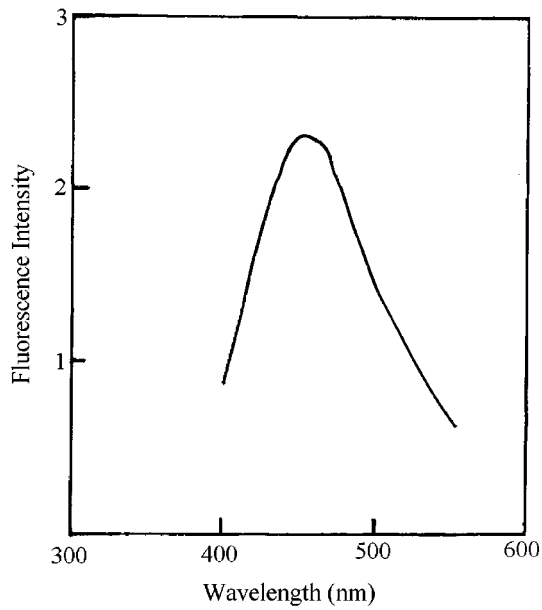

FIG. 6. PL spectrum of ZnS nanocrystallites ($\lambda_{ex} = 350$ nm).

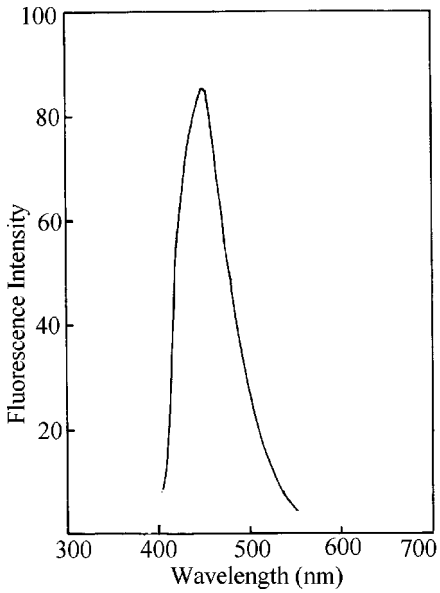

FIG. 7. PL spectrum of pure glass sample (heat-treated at 50°C, $\lambda_{ex} = 380$ nm).

luminescent processes are increased. Thus, the relative fluorescence intensity of the doped samples decreases with increasing impurity mole ratios when the impurity mole ratios of doped ions exceed certain values. When the impurity mole ratios of Ni^{2+} and Mn^{2+} exceed 0.3% and 0.5%, respectively, the relative fluorescence intensities of Ni^{2+}- and Mn^{2+}-doped samples decrease with increasing impurity mole ratio of Ni^{2+} and Mn^{2+}.

Figure 10 shows the emission spectra of the glass samples co-doped with Ni^{2+} and Mn^{2+} (heat-treated at 50°C, $\lambda_{ex} =$ 380 nm). The excitation wavelength of the co-doped samples is 380 nm. All of the co-doped samples show emission peaks almost at the same position. However, the co-doping shifts the luminescent peak to 420 nm. The relative fluorescence intensity of co-doped samples is weaker than that of Ni- and Mn-doped samples.

Usually, two emissions are observed from luminescent materials—excitonic and trapped luminescence (18). The excitonic emission is sharp and is located near the absorption edge of the materials while the trapped emission broad and is Stokes-shifted. The results show that the doped and undoped samples have broad emission bands. Only the trapped luminescence arising from the surface states is observed in the doped and undoped samples. Therefore, the excitation spectrum of the doped samples is almost the same as that of the undoped sample although the doped samples have different absorption shoulder and absorption edge.

To understand the structure and formation mechanism of defect in sol–gel silica glass has become a subject of con-

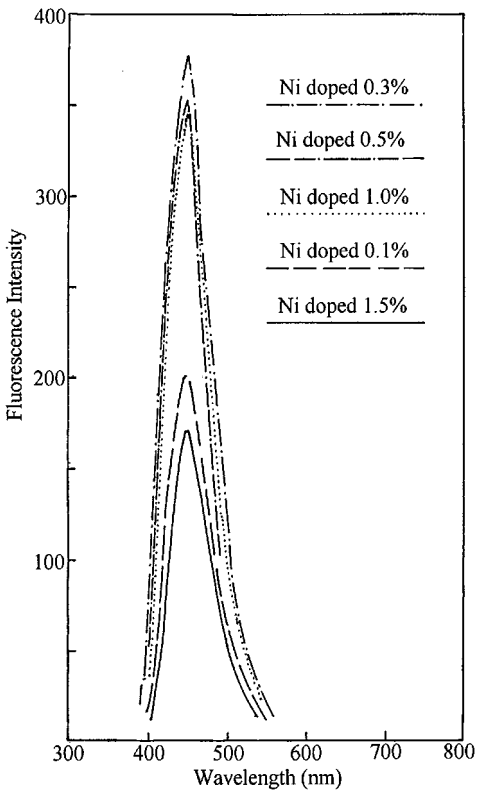

FIG. 8. PL spectra of the Ni^{2+}-doped samples (heat-treated at 50°C, $\lambda_{ex} = 380$ nm).

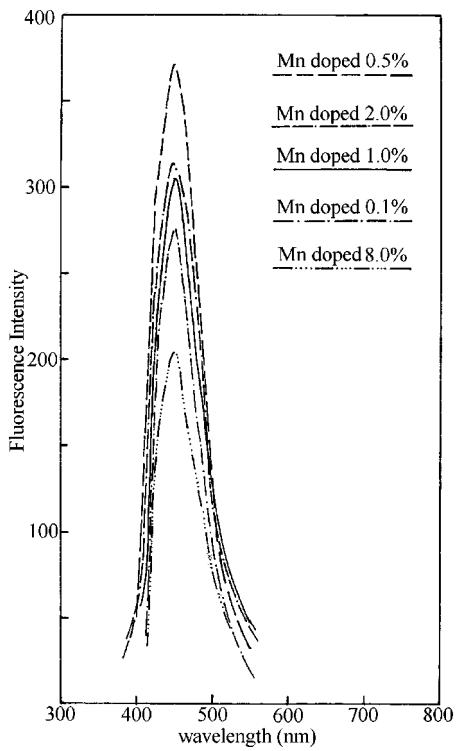

FIG. 9. PL spectra of the glass samples doped with Mn^{2+} ($\lambda_{ex} = 380$ nm, mean impurity mole ratio).

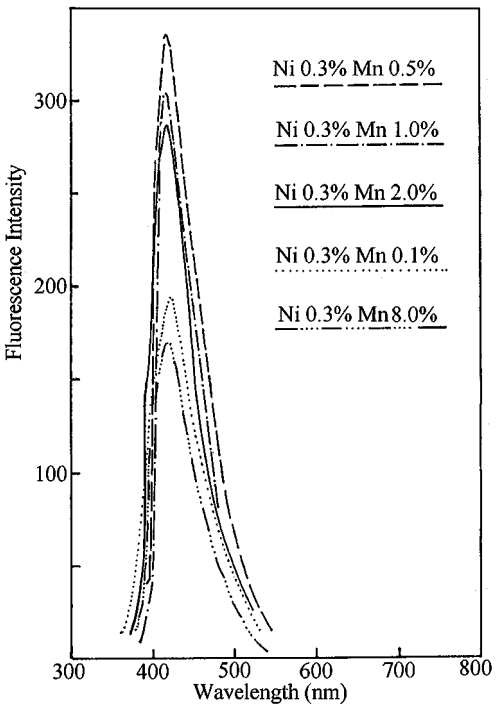

FIG. 10. PL spectra of the glass samples co-doped with Ni^{2+} and Mn^{2+} (λ_{ex} = 380 nm, mean impurity mole ratio).

siderable interest since amorphous silicon dioxide is an indispensable material component of fiber-optic technologies and metal-oxide-semiconductor devices (11, 12). The sol–gel SiO_2 glass is a porous phosphor material. Because it is a porous material and has many defects, it can show a variety of luminescent behaviors (common SiO_2 glass do not show PL) (4). The fluorescence efficiency of the sol–gel glass increases with increasing defects in the silica glass network. In the system of $Si(C_2H_5O)_4$–enthonol–H_2O, the reaction formed SiO_2 glass network is from hydrolysis–condensation polymerization: $n\mathrm{Si(OR)_4} + 2n\mathrm{H_2O} \rightarrow n\mathrm{SiO_2} + 4n\mathrm{ROH}$. G. Exeline *et al.* first examined the general consequences that follow photoexcitation of a solid to establish the basis of the discussion for wide band gap solids (such as ZrO_2 powder and xerogel) (16). The outcome is best illustrated by a set of quasi-chemical reactions (16):

$$\mathrm{L} + h\nu_1 \rightarrow e^{\circ} + (e + h) \qquad [1a]$$

$$\mathrm{D} + h\nu_2 \rightarrow e + \mathrm{D} + \text{ or } h + \mathrm{D}^- \qquad [1b]$$

$$\mathrm{L_s} + h\nu_1 \rightarrow e_s^{\circ} + (e_s + h) \qquad [1c]$$

$$\mathrm{S} + h\nu_2 \rightarrow e_s + \mathrm{S}^+ \text{ or } h_s + \mathrm{S}^-. \qquad [1d]$$

The first step (Eq. [1a]) represents an intrinsic, i.e., fundamental absorption by the bulk lattice L with photon energy $h\nu_1$ that produces free exciton and free charge carriers e and h; the second step (Eq. [1b]) denotes light absorption by bulk lattice defects D (for example, the absorption associated with intrinsic lattice defects and/or impurities) with $h\nu_2 < h\nu_1$ also to give free carriers and the photoionized defect states D^+ or D^-. Photoexcitation of the regular lattice surface, L_s (step 1c), generates surface excitions, electrons, and holes. Light absorption by surface defects in Eq. [1d] (ion vacancies, surface ions of low coordination number at corners, edges, or terraces) or by surface impurities S yields surfaces active with donor and acceptor molecules, respectively (16). Therefore, the luminescence mainly comes from the bulk lattice L, the bulk lattice defects D, surface defects S, and the surface state L_s of wide band gap solids.

In the hydrolysis–condensation polymerization of the $Si(C_2H_5O)_4$–ethanol–H_2O system, because the reaction rate is fast and the hydrolyzed reaction is not being carried out completely, there are a large number of defects in the SiO_2 glass network in the primary step. They may be $\equiv Si^{\bullet}$, $=Si^{\bullet\bullet}$, $\equiv Si\text{–}O^{\bullet}$, $\equiv Si\text{–}OH$, $\equiv Si\text{–}OC_2H_5$, $\equiv Si\text{–}Si\equiv$ and others. Because the reaction is in acid solution, the defects ($\equiv Si\text{–}OH$, $\equiv Si\text{–}OC_2H_5$) are reduced with the processes of reaction: $\equiv Si\text{–}OH + H^{\bullet} \rightarrow \equiv Si^{\bullet} + H_2O$; $\equiv Si\text{–}OC_2H_5 + H^{\bullet} \rightarrow \equiv Si^{\bullet} + C_2H_5OH$. Therefore, the three-dimensional network of the sol–gel glass is not well-distributed and ordered. The porous sol–gel SiO_2 glass includes a lot of Si dangling bonds, nonbridging oxygen, and oxygen vacancy, well-distributed in its structure and inside surface of nanometer-scale holes (14, 15). The defects induced a very strong visible light luminescence in the sol–gel silica glass. The Si dangling bond, nonbridging oxygen, and oxygen vacancy are assumed to be the luminescent species for strong blue-purple emission of the sol–gel porous silica glass:

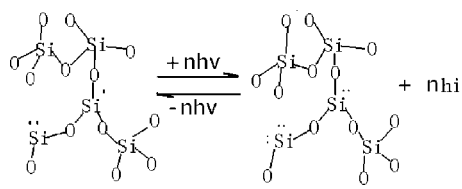

[2]

Due to the large number of nanometer-scale holes (15–100 Å) in the sol–gel silica glass (17), the inside surface defects also affect the luminescence properties of the sol–gel silica glass.

The asymmetric PL bands of the transition-metal ions are assigned to their *d–d* transition. In ZnS semiconductor materials, the lowest multiplet term ^3F of the free Ni^{2+} ion is split into $^3T_1$, $^3T_2$, and $^3A_2$ through anisotropic hybridization. Due to the *d–d* optical transitions of Ni^{2+}, the luminescent center of Ni^{2+} is formed in ZnS (20). Thus, green luminescence has been observed from Ni^{2+}-doped samples. The first excited multiplet term ^4G of the free

Mn^{2+} (d^5) is split into $^4T_1$, $^4T_2$, $^4A_1$, and ^4E. The emission wavelength of Mn^{2+}-doped ZnS nanometer-scale semiconductor materials may be from yellow to orange. The orange emission of Mn^{2+} in ZnS nanocrystallites is due to the d–d ($^6A_1$ (^6S)–$^4T_2$ (^4G)) transition of Mn^{2+}. The yellow emission of Mn^{2+} in ZnS nanocrystals is due to the d–d ($^4T_1$–$^6A_1$) transition of Mn^{2+} (19). Therefore, the matrix materials affect the d–d transition of the transition-metal ion. The doped ions have different luminescence spectra in different matrix materials. On the other hand, the doped ions (Ni^{2+} and Mn^{2+}) can affect the band gap structure of the matrix. The doped ions can change the luminescence properties of the host materials. In the samples co-doped with Ni^{2+} and Mn^{2+}, the doped ions can lead to formation of more Si dangling and oxygen vacancy in the network of the silica glass. More excited easily electrons or holes and radiative combinations are increased. On the other hand, the band gap structure of co-doped samples is different from those of Ni^{2+}- and Mn^{2+}-doped samples and undoped sample. Because of the complication of transitions from the conduction band to the ground-state level of the Ni^{2+} and Mn^{2+} luminescent centers and the structure defects of the silica glass, the emission wavelength of the co-doped samples is remarkably different from those of Ni^{2+}- and Mn^{2+}-doped samples. Therefore, the emission wavelength of the co-doped samples has blue shifted.

The enhancing mechanism of the luminescence of Ni^{2+}- and Mn^{2+}-doped samples has two aspects. First, because Ni^{2+} and Mn^{2+} ions are not network formation bodies, Ni^{2+} and Mn^{2+} ions can be interstitial ions in the sol–gel SiO_2 glass network. They may be associated by nonbridging oxygen. Therefore, Ni^{2+} and Mn^{2+} ions can increase the concentration of the Si dangling bond. Ni^{2+} and Mn^{2+} ions increase the surface defects inside of the nanometer-scale hole. Thus, more electrons and holes are excited. The radiative combination is dramatically increased. The fluorescence efficiencies of the samples doped with Ni^{2+} or Mn^{2+} are remarkably increased over those of the undoped samples. Second, according to our experimental results, the emission band of the luminescent centers of Ni^{2+} or Mn^{2+} ions in the silica glass is almost the same as those of undoped samples. Therefore, the relative fluorescence intensities of Ni^{2+}- and Mn^{2+}-doped samples increase over those of the samples co-doped with Ni^{2+} and Mn^{2+}.

CONCLUSION

The sol–gel SiO_2 glass doped with transition metal ions shows a novel PL property. The PL characteristics of a kind of metal-ion-doped sol–gel glass are different from those of co-doped and undoped samples. The fluorescence efficiencies of the sample doped with Ni^{2+} or Mn^{2+} are about 4 times of those of the pure glass samples. Their emission wavelength is almost the same as that of the undoped glass sample ($\lambda_{em} = 450$ nm). Because the surface defects and the concentrations of Si dangling bond, oxygen vacancy, nonbridging oxygen, etc. are increased in the doped sample, the fluorescence efficiencies of doped samples are remarkably increased. The co-doping of Ni^{2+} and Mn^{2+} results in a blue shift of the emission wavelength of the co-doped samples. The fluorescence intensity of the co-doped samples is weaker than that of Ni^{2+}- and Mn^{2+}-doped samples.

ACKNOWLEDGMENTS

The authors thank the Natural Science Foundation of China for support (69890230).

REFERENCES

1. N. Chiodini, F. Meinardi, F. Morazzoni, A. Paleari, R. Scotti, and D. Di Martino, *Appl. Phys. Lett*. **76,** 3209–3211 (2000).
2. L. H. Slooff, M. J. A. de Dood, A. Van Blaaderen, and A. Polman, *Appl. Phys. Lett*. **76,** 3682–3684 (2000).
3. W. H. Green, K. P. Le, J. Grey, T. T. Au, and M. J. Sailor, *Science* **276,** 1826–1828 (1997).
4. S. Okuzaki, K. Okude, and T. Ohishi, *J. Non-Cryst. Solids* **265,** 61–67 (2000).
5. A. Ibanez, S. Maximov, A. Guiu, C. Chaillout, and P. L. Baldeck, *Adv. Mater*. **10,** 1540–1543 (1998).
6. D. Zhao, W. Li, Z. Hong, X. Liu, C. Liang, and D. Zhao, *J. Lumin*. **82,** 105–109 (1999).
7. M. Nogami and Y. Abe, *Appl. Phys. Lett*. **65,** 2545–2547 (1994).
8. L. Liao, X. Bao, X. Zheng, N. Li, and N. Min, *Appl. Phys. Lett*. **68,** 850–852 (1996).
9. G. Irmer, J. Monecke, P. Verma, G. Goerigk, and M. Herms, *J. Appl. Phys*. **88,** 1873–1879 (2000).
10. N. Lopez, F. Illas, and G. Pacchioni, *J. Phys. Chem. B* **104,** 5471–5477 (2000).
11. M. D. Curran and A. E. Stiegman, *J. Phys. Chem. B* **104,** 8338–8345 (2000).
12. T. Uchino, M. Takahashi, and T. Yoko, *Phys. Rev. B* **62,** 2983–2986 (2000).
13. R. Vacassy, S. M. Scholz, J. Dutta, and C. J. G. Plummer, *J. Am. Ceram. Soc*. **81,** 2699–2703 (1998).
14. H. Imai, K. Arai, H. Imagawa, H. Hosono, and Y. Abe, *Phys. Rev. B* **38,** 12772–12775 (1998).
15. G. Pacchioni and G. Ierano, *Phys. Rev. Lett*. **79,** 753–757 (1997).
16. G. Exeline, G. V. Kataeva, A. S. Litke, A. V. Rudakova, V. K. Ryabchuk, and N. Serpone, *Langmuir* **14,** 5011–5022 (1998).
17. B. J. Loughnane, R. A. Farrer, A. Scodinu, T. Reilly, and J. T. Fourkas, *J. Phys. Chem. B* **104,** 5421–5429 (2000).
18. W. Chen, Z. Wang, Z. Lin, and L. Lin, *Appl. Phys. Lett*. **70,** 1466–1470 (1997).
19. K. Sooklal, B. S. Cullum, S. M. Angel, and C. J. Murphy. *J. Phys. Chem*. **100,** 4551–4555 (1996).
20. P. Yang, M. K. Lu, D. Xu, D. Yuan, J. Chang, G. J. Zhou, and M. Pan, *Appl. Phys. A* (2001), in press.
21. M. Jain, "II–VI Semiconductor Compounds," pp 105–120, World Scientific, Singapore, 1994.